NASA/CR-1998- 207561

Use of Microgravity to Control the Microstructure of Eutectics

NASA Grant NAG8-1266
Progress report: 1 March 1998

IN-26-CR
078033

Co-Principal Investigators: William R. Wilcox and Liya L. Regel
Clarkson University, Potsdam NY 13699-5814
Co-Investigator: Reginald W. Smith
Queen's University, Kingston, Ontario
Technical Contract Monitor: Barbara Facemire
NASA Marshall Space Flight Center
Graduate research assistants: Dmitri Popov (Engineering Science PhD student)
Fengcui Li (Chemical Engineering PhD student)
Ram Ramanathan (Chemical Engineering MS student)

ABSTRACT

This grant began in June of 1996. Its long term goal is to be able to control the microstructure of directionally solidified eutectic alloys, through an improved understanding of the influence of convection. The primary objective of the present projects is to test hypotheses for the reported influence of microgravity on the microstructure of three fibrous eutectics (MnBi-Bi, InSb-NiSb, Al3Ni-Al). A secondary objective is to determine the influence of convection on the microstructure of other eutectic alloys.

Two doctoral students and a masters student supported as a teaching assistant were recruited for this research. Techniques were developed for directional solidification of MnBi-Bi eutectics with periodic application of current pulses to produce an oscillatory freezing rate. Image analysis techniques were developed to obtain the variation in MnBi fiber spacing, which was found to be normally distributed. The mean and standard deviation of fiber spacing were obtained for several freezing conditions. Eighteen ampoules were prepared for use in the gradient freeze furnace QUELD developed at Queen's University for use in microgravity. Nine of these ampoules will be solidified soon at Queen's in a ground-based model. We hope to solidify the other nine in the QUELD that is mounted on the Canadian Microgravity Isolation Mount on MIR.

Techniques are being developed for directional solidification of the Al-Si eutectic at different freezing rates, with and without application of accelerated crucible rotation to induce convection.

For the first time, theoretical methods are being developed to analyze eutectic solidification with an oscillatory freezing rate. In a classical sharp-interface model, we found that an oscillatory freezing rate increases the deviation of the average interfacial composition from the eutectic, and increases the undercooling of the two phases by different amounts. This would be expected to change the volume fraction solidifying and the fiber spacing. Because of difficulties in tracking the freezing interfaces of the two solid phases, a phase-field model is also being developed. A paper demonstrating application of phase field methods to periodic structures has been submitted for publication.

INTRODUCTION

Prior experimental results on the influence of microgravity on the microstructure of fibrous eutectics have been contradictory [reviewed in 1,2]. Theoretical work at Clarkson University showed that buoyancy-driven convection in the vertical Bridgman configuration is not vigorous enough to alter the concentration field in front of a growing eutectic sufficiently to cause a measurable change in microstructure [3-9]. Currently, there are three hypotheses that might explain the observed changes in microstructure of fibrous eutectics caused by convection:

1. A fluctuating freezing rate, combined with unequal kinetics for fiber termination and branching.
2. Off-eutectic composition.
3. Presence of a strong habit modifying impurity.

We favor the first of these hypotheses. Previously we had performed ground-based experiments using electric current pulses to deliberately create an oscillatory freezing rate [1,2]. Although current pulsing coarsened the microstructure of MnBi-Bi eutectic as predicted, it may also have introduced localized convection. Current pulsing experiments in microgravity are needed to fully test this hypothesis.

Experimental and theoretical research is being carried out in collaboration with Professor Reginald Smith of Queen's University. He is a senior metallurgist with extensive experience in eutectic solidification, including the two systems being investigated here: MnBi-Bi and Al-Si. Through the support of the Canadian Space Agency, he has two automated furnaces located in the Canadian Microgravity Isolation Mount (MIM), in Prirorda on *Mir*. MIM can be used not only to greatly reduce acceleration, it can also be used to introduce accelerations of any desired amplitude, frequency and direction. Recent experiments have shown unexpected sensitivity of diffusion to normal microgravity g-jitter [10,11]. Thus it would be very instructive to perform eutectic solidification experiments in microgravity with controlled accelerations applied, either using MIM or McDonnell-Douglas's STABLE.

ACKNOWLEDGMENTS

We are very grateful to Ms. Barbara Facemire for her interest and encouragement, and for arranging use of the supercomputer at Marshall Space Flight Center. Bill Plunkett provided valuable assistance with use of the scanning electron microscope at Clarkson University.

THE INFLUENCE OF A FLUCTUATING FREEZING RATE ON DIRECTIONAL SOLIDIFICATION OF THE MnBi/Bi EUTECTIC

Fengcui Li

Abstract

The objective of this project is to determine the effect of a fluctuating freezing rate on the microstructure of the MnBi/Bi eutectic. It was planned that this would be done via both space experiments and ground-based experiments. The space experiments were to be carried out in collaboration with Professor Reginald Smith of Queen's University. Through the support of the Canadian Space Agency, he has two automated furnaces located in the Canadian Microgravity Isolation Mount (MIM), in Prirorda on Mir. At Clarkson, ground-based experiments are being performed with a fluctuating freezing rate caused by passing periodic electric current pulses through the material. Experiments will be carried out soon at Queen's University using duplicates of the flight samples in a copy of the flight furnace, QUELD. Eighteen special small diameter ampoules were prepared and delivered to Professor Smith. Because of the many problems with Mir, flight of our experiments is now awaiting the negotiation of a new agreement between the Canadian Space Agency and the Russian government.

The eutectic microstructure is photographed using Scanning Electron Microscopy (SEM), and the microstructure images analyzed by special image analysis software that we do not believe has been used before in such an application. The result is a histogram of the distribution of nearest neighbor MnBi rod spacings. Cumulative distribution plots demonstrate that this rod spacing is normally distributed.

A draft research proposal by Ms. Li for her PhD qualifying examination is nearly complete. There has been an introductory meeting with the examining committee.

INTRODUCTION

The MnBi/Bi eutectic has potential for use in the production of permanent magnets. It provides a fine dispersion of ferromagnetic MnBi embedded in a diamagnetic Bi matrix. Regular arrays of MnBi rods are aligned with their easy axis of magnetization parallel to the growth direction in the Bi matrix. Moreover, MnBi/Bi eutectic is considered a useful model system to study the crystal growth, because its microstructure and magnetic properties strongly depend on the solidification parameters.

The average MnBi fiber spacing λ depends on the freezing rate V such that $\lambda^2 V = \text{const}$. In the 1980's, Larson and Pirich at Grumman found that λ of MnBi/Bi solidified in microgravity was reduced to about half the value when it is solidified on earth [reviewed in 1,2]. However, a more recent flight experiment by Smith showed no influence on the microstructure of MnBi/Bi eutectic. Previous investigations here showed that the influence of buoyancy-driven convection and the Soret effect on mass transport are not enough to explain the difference between the earth- and space-processed [3-9]. We proposed that freezing rate fluctuations caused by irregular convection increased λ on earth because MnBi fibers are terminated more easily than they branch. We also proposed that the difference between the results of Larson and Smith resulted from the different temperature profiles of their experimental apparatuses. The thermally unstable condition of Larson's furnace is believed to have caused time-dependent convection, temperature fluctuations and freezing rate fluctuations. (They observed temperature fluctuations via thermocouples in the melt.) Smith used a thermally stable gradient-freeze furnace.

The objective of the current project is to experimentally determine the influence of a fluctuating freezing rate on the microstructure of the MnBi-Bi eutectic. Ground-based experiments are being performed at Clarkson using periodic electric current pulses applied during solidification. Electric current pulsing is a good technique to cause rapid freezing rate fluctuations, hopefully with minimum changes to the convection. In preliminary experiments, we demonstrated that the MnBi fiber spacing increased as both the current amplitude and duration were increased at one particular freezing rate [1,2]. We are now investigating a range of freezing rates and current pulsing conditions.

We plan to perform experiments soon at Queen's University on a duplicate of the QUELD gradient-freeze apparatus that is located on the Canadian Microgravity Isolation Mount (MIM) on Mir. Perturbations will be induced in some of the 9 experiments by orienting the apparatus horizontally during solidification or by periodically striking the apparatus. Ultimately, we hope to perform solidification experiments on MIM in space, under three conditions: without vibration damping, with vibration damping, and with known oscillations applied by MIM. (Diffusion studies have shown that g-jitter on the Shuttle and on MIR are sufficient to increase the apparent diffusion coefficient compared to the vibration-damped condition [10,11].) The problems on MIR have prevented our samples from being run, and we must now await the negotiation of a new agreement between the Canadian Space Agency and the Russian authorities.

EXPERIMENTAL METHODS, RESULTS AND PLANS

Current pulsing experiments

The experimental procedure is as follows. The ampoules used for homogenization are 9 mm ID× 11 mm OD quartz tubes, sealed by 8 mm OD quartz rods on both ends. The ampoule was alternately evacuated to 10^{-6} torr and filled with a mixture of argon and 10% hydrogen, and then sealed at 10^{-6} torr. The eutectic was homogenized in the gold-coated rocking furnace at 670°C for 36 hours.

The growth ampoules are 4 mm ID X 6 mm OD quartz tubes (with 9 mm ID X 11 mm OD top parts), and 900 mm long in order to fit the furnace. Molybdenum wire is used to carry the electric current for the current pulsing experiments since it is not soluble in bismuth. The charge is about 20 g, and the ingot length is about 15 cm.

A Bridgman-Stockbarger furnace is used for the solidifications. The temperature in the hot zone is set at 650°C and the cold zone at 250°C. A current amplitudes of about 0, 1, 5 and 9 A is used, i.e. 8.0, 40 and 72 A/cm^2. The period is 2s, 6s or 40s. The duration time is about 12.5%, 25% and 50% of the period time. Some experiments are performed either with no current or with current applied continuously. The translation rate, which is approximately the freezing rate, is 1, 2 or 5 cm/hr. For most ingots, no current is used during the first 6 cm, 9 A for 3 cm, 5A for 3 cm and 1A for 3 cm. Ampoules successfully solidified to date are shown in the table at the end of this section.

Each ingot is cut into 8 mm thick cross sections, which are mounted in epoxy, ground, polished and etched. The microstructure is recorded as computer files using scanning electron microscopy. For each sample, 20-25 images from different positions of the sample are saved and subsequently analyzed by HLImage++ 97 software. By the Threshold and Blob Analyse command, the edge between the rods and the matrix are found. Some images are not sharp enough and are fixed manually using the image software. Each rod area and center coordinates are obtained automatically by the computer. The results are exported to Excel. The rods are sorted from largest to smallest. There are four items in the Excel table for each rod: its

identification number, area, and coordinates of its center. The distance of its center to that of the nearest rod is calculated and stored. The average nearest-neighbor spacing is calculated and defined as the rod spacing λ, along its standard deviation and total fraction of the area occupied by MnBi fibers (area fraction). The nearest-neighbor values are used to generate a frequency histogram, as illustrated in the graph shown later. The cumulative distribution is tested for normalcy by a plot of nearest neighbor distance versus the standard normal cumulative distribution function NORMSINV. A straight line, as illustrated in the graph on the last page of this section, indicates that the nearest neighbor distance is normally distributed. The 50% value on this plot is λ and the slope is the standard deviation.

QUELD experiments

The Queen's University flight furnace, QUELD, is a gradient freeze furnace designed to hold one sample. The control temperature is lowered at a specified rate to cause directional solidification. Eighteen ampoules were prepared for use with QUELD, 9 for ground-based experiments and 9 for flight experiments. Each ampoule is 3 mm ID $\times$ 5 mm OD and 60 mm long quartz tube, with its two end sealed by fusing in quartz rods. These 18 ampoules were delivered to Professor Smith and we are now collaborating with him on selection of the conditions for the 9 ground-based experiments. We believe some will be run vertically in a thermally stable environment, and some horizontally to cause convection and a fluctuating freezing rate. We are considering periodically tapping the furnace in order to cause the freezing rate to fluctuate. This could be done either manually or by using a rotating cam or solenoid.

Overview of the experiments

No.	EX1	EX2	EX3	EX4	EX5	EX6	EX7
Charge(g)	40.0	50.0	17.0	22.1	22.0**	20.8**	22.1**
C_{Mn}(wt%)	0.726	0.737	0.721	0.738	0.730	0.738	0.738
Ampoule size (mm)	9 ID 11 OD	9 ID 11 OD	4 ID 6 OD	4 ID 6 OD	4 ID 6 OD	4 ID 6 OD	4 ID 6 OD
Ingot length (cm)	6.8	8.8	12.0	leaked oxidized	18.0	17.3	18.2
Soak time (hr)	3.25	3.50	2.50	2.50	2.75	3.30	4.50
Translation rates (cm/hr)	1.88	1.92	6.75, 4.09, 2.07, 0.83	2.0	2.10	2.14	4.36
Current settings*	No current	No current	No current	I = 9A t = 1s T = 2s	I = 0, 9, 5, 1A; t = 0.75s; T = 6s	I = 0, 5, 1, 9A; t=1s; T=2s	I = 0, 9, 5, 1A t = 0.5; T = 2s; constant 5A
SEM analysis	Yes	Yes	Yes				
Area Fraction	3%	3%	3.0,2.7, 4.5,5.6%				
Average λ(μm)	4.6	4.5					
Standard deviation	1.51μm	1.02μm					

* I: current amplitude t: current duration time T: period of the current pulses
** The charge was a 3mm OD ingot that had been solidified in a 3mm ID × 5mm OD quartz tube.

Explanation of the experiments

No.	Explanation
EX3	The crystal was solidified in four translating rates. The ingot lengths were 4.5, 3.0, 3.0, 2.0cm.
EX5	The crystal was solidified in five conditions. First 4cm long was grown without current pulses. Then l=3.5cm at each current pulses. The last 3.3cm without current
EX6	l_1=4.6cm with I=5A; l_2=2.4cm no current; l_3=3.7cm with I=1A; l_4=2.2cm without current; l_5=3.8cm with I=9A; The last part was solidified without current
EX7	l_1=3.3cm no current; l_2=3.4cm with I=9A; l_3=3.2 with I=5A; l_4=3.2cm with I=1A; l_5=2.8cm with I=5A constant current; The last part was solidified without current

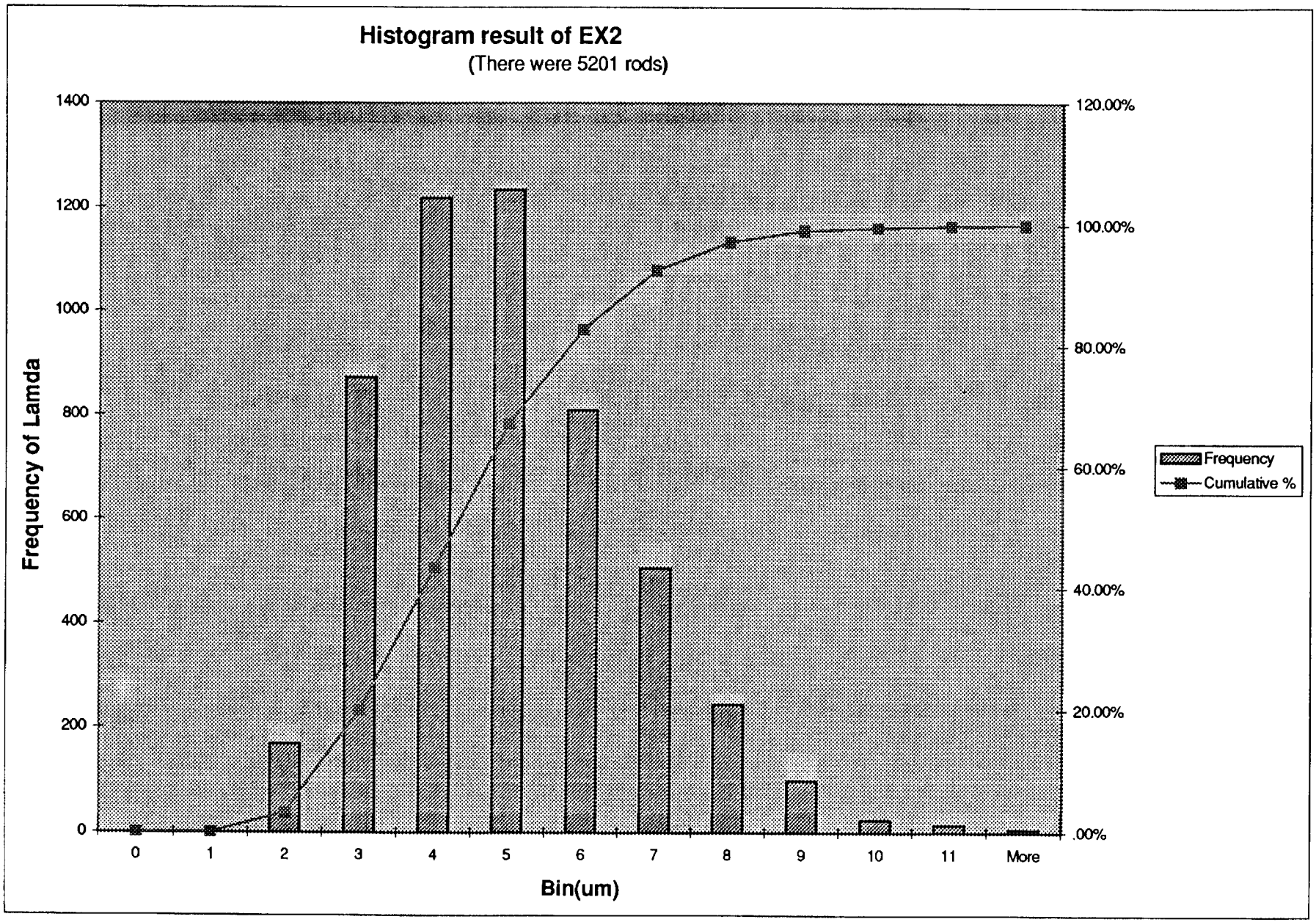
Histogram result of EX2
(There were 5201 rods)
Frequency of Lamda
1400
1200
1000
800
600
400
200
0
120.00%
100.00%
80.00%
60.00%
40.00%
20.00%
.00%
0
1
2
3
4
5
6
7
8
9
10
11
More
Bin(um)
Frequency
Cumulative %

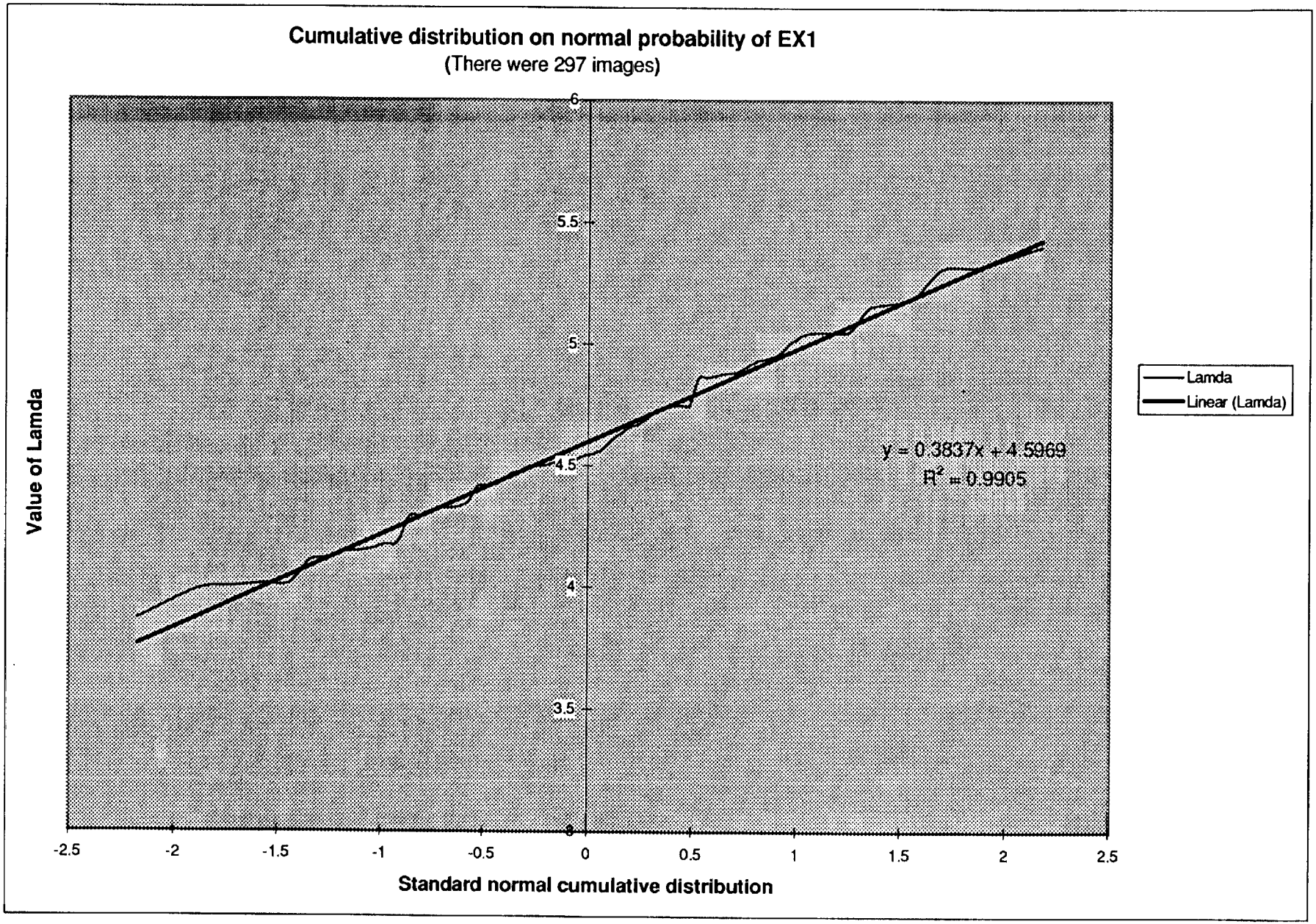
Cumulative distribution on normal probability of EX1
(There were 297 images)
Value of Lamda
6
5.5
5
4.5
4
3.5
3
-2.5
-2
-1.5
-1
-0.5
0
0.5
1
1.5
2
2.5
Standard normal cumulative distribution
Lamda
Linear (Lamda)
y = 0.3837x + 4.5969
R² = 0.9905

MODELING OF EUTECTIC SOLIDIFICATION WITH A FLUCTUATING FREEZING RATE

Dmitri Popov

Abstract

It was proposed in [1,2] that the kinetics of fiber branching differs from that for fiber termination. This could explain why the fiber spacing λ is different when solidification is carried out without freezing rate fluctuations caused by buoyancy-driven convection. The objective of this project is to develop a theoretical model for the influence of freezing rate oscillations on eutectic microstructure. We are unaware of any previous work in this area. Two different numerical models were chosen to solve the problem:

One-sided model. This method is based on the solution of thermal and mass diffusion equations separately in each phase and sewing the solution at the interface by appropriate boundary conditions resulting from flux conservation. The equations in the bulk can be easily discretized even in a very complicated geometry. The interfacial free energy cannot be calculated from the model, but is formulated in the model *ab initio*. In this case, the dynamics of the interface is controlled only by the change of field variables in the bulk, but not at the interface itself. A fluctuating freezing rate was applied. The coordinate system was transformed to one moving with the interface. The excess compositional undercooling was calculated for several eutectic structures. It was found that the stationary solution always exists. The concentration at the interface, averaged in the Jackson-Hunt fashion, oscillates with the same frequency as the growth rate, but lags behind for sufficiently high frequencies. The frequency dependence of the average compositional undercooling reveals a high-frequency cut-off, where it approaches the steady-state value. The value of the high-frequency cut-off is proportional to the inverse diffusion time connected with the lateral diffusion. The value of the liquidus slope at the eutectic point of the phase diagram turns out to be important for the estimation of the excess undercooling buildup at the interface.

Phase-field model. In order to be able to track the interface dynamics, and particularly the region of connection of the three phases (liquid and two solid phases), we initially chose the phase-field method. The governing equations were formulated using two phase-field parameters, functions of temperature and concentration. First, the necessary accuracy in the calculations of the concentration in the bulk of the phases was achieved in one dimension and one solid phase, providing the correct solution for the interfacial region. A fluctuating freezing rate and concentration ahead of the interface were obtained as a response to a temperature fluctuation at the edge of the thermal boundary layer. The concentration also lags behind the interface velocity fluctuation as in the one-sided model. A simple lamellar eutectic structure was recovered in a constant temperature gradient. The interface shape and the composition field ahead of the interface are in agreement with Jackson-Hunt speculations [12].

INTRODUCTION

In studying the influence of a fluctuating freezing rate on MnBi/Bi eutectic solidification, a series of experiments were accomplished at Clarkson [13]. Fu and Wilcox [14-16] studied heat transfer in the Bridgman-Stockbarger technique with a sudden change in translation rate. Both

experimentally and theoretically they showed that that the freezing rate does not immediately equal the new translation rate, but rather approaches it asymptotically. In such a situation, the microstructure of MnBi/Bi eutectic always corresponded to the instantaneous freezing rate, i.e. the microstructure adapted more quickly than heat transfer allowed the freezing rate to change.

When the freezing rate V increases, the system wants the MnBi fiber spacing λ to decrease in order to maintain $\lambda^2 V$ constant. In fiber eutectics, this probably occurs by branching of existing fibers, perhaps by nucleation of another orientation. Because MnBi is faceted, branching seems to occur with considerable difficulty. Consequently, we hypothesize that the microstructure lags behind the velocity change until the freezing rate begins to decrease. With a decreasing freezing rate, the system wants λ to increase. This is probably accomplished by the Bi matrix growing around and pinching off fibers. Apparently, in the Mn-Bi system this occurs more readily than does branching. The net effect of this mechanism would be to yield a λ that always exceeds the value expected for the average freezing rate.

Regel and Wilcox [1,2] also proposed that fiber branching is easier than fiber termination in some systems. They took as an example fibers that extend out in the melt a long distance in front of the matrix. This could explain why, for one fibrous eutectic, λ increased when solidification was carried out in space. They observed that the above mechanism is probably not relevant to lamellar eutectics, for which λ adjusts by propagation of faults. Previous work showed that solidification in microgravity and use of ACRT had no influence on the λ of lamellar eutectics. However, solidification is no longer at steady state when the freezing rate is fluctuating. Consequently, the volume fractions of the two phases and their average interfacial undercooling may depart from steady state values.

Thus, the results of Larson and Pirich are not surprising, but cannot be understood using steady state theories. A quantitative theory of oscillatory freezing is needed for comparison with experiment. There was no directly related prior work on this subject. There have been a number of works on the morphological stability of lamellar eutectics.

Linear analytical analyses and numerical solutions have been carried out to find out the stability of a freezing interface subjected to perturbations. Hurle, Jakeman and Pike [17] investigated the effect of sinusoidal temperature variations in the melt on the growth of a single-phase crystal. They solved the concentration-diffusion and heat-conduction equations for both solid and liquid phases in linear approximation in 1 dimension. They imposed a sinusoidal temperature perturbation of frequency ω at the edge of the thermal boundary layer adjacent to the advancing phase boundary. The response of the temperature and concentration at the interface was calculated. The authors showed how these quantities vary with frequency for material parameters appropriate to metals and semiconductors.

Wilson [18] investigated the quantitative relationship between periodic variations in growth rate and compositional inhomogeneities in single-phase crystals grown by the Czochralski technique. Using an extension of the Burton-Prim-Slichter model, she solved numerically the Navier-Stokes equation, the continuity equation and the diffusion equation. These calculations indicated that the concentration cycle at the interface lags the growth rate cycle. The general form of the parametric dependence of the phase lag was not obtained. It was only noted that, because of the phase lag effect, the concentration profile is non-symmetric about its maxima and minima. The time-dependent variation in concentration in the melt at the interface was established.

Wheeler [19] also used a linear stability theory to study the effect of an oscillatory growth rate on the morphological stability of a crystal growing from a binary alloy in 2 dimensions. The

oscillatory component was assumed to be less than the average freezing rate, and the solute diffusivity in solid phase much less then in liquid phase.

Until now, no calculations had been done for a eutectic system, either lamellar (2-dimensional) or fibrous (3-dimensional), with a fluctuating freezing rate caused by temperature oscillations in the melt.

METHODS

Analytical methods seemed to be inappropriate for this problem. Even if the governing equations for temperature and composition fields are uncoupled, there is a time-dependent freezing rate, which makes the problem non-linear. A numerical solution can be compared either with simplified analytical models or with an order-of-magnitude analysis.

One-sided sharp interface model

The choice of a numerical method to solve this problem is based mainly on the results one wants to accomplish. For moving interface problems, the dilemma is in the interface approximation. If only the bulk of the phase is of interest, then the interface is approximated by a surface (line in a 2-dimensional case) in the mathematical sense, i.e. with zero width. The equations in the bulk can be easily discretized even in a very complicated geometry. Domain decomposition methods have been extensively used to study the cellular growth problem [20,21]. However, the method still relies partially on domain transformation (mapping), which is hardly applicable for highly contorted interfaces. The effectiveness of the method is diminished by the necessity of periodic reconnection of grids and consequent interpolations, which may result in numerical diffusion. Their formulation is akin to the method proposed by Shyy *et al.* [22]. A deficiency in these methods is their inability to describe the interface. The dynamics of the interface is controlled only by the change of field variables in the bulk, but not at the interface itself.

We consider a system of two-dimensional elliptic equations which describe the evolution of concentration and temperature field in three-phase two-component media. Having assumed that in the solid phases the thermal diffusivities are equal and the mass diffusivities 0, we end up with a system of three differential equations describing concentration evolution in the liquid phase and temperature evolution in the solid and liquid phases. Here, we are assuming that the solid/liquid interface is planar for each phase, but the phases can have different kinetics of propagation. Initially, for simplicity we assumed that the growth velocity is the same for both phases. The interface propagates in the z-direction, with the x-direction being the direction of eutectic structure periodicity. The equations are coupled by means of boundary conditions applied at the propagating solid/liquid interface.

The relevant physical scaling for this problem, where the mass diffusion plays an important role, can be assessed by introducing the average growth rate V_0, mass diffusivity D and eutectic structure parameter:

$$z = \tilde{z}\frac{D}{V_0} \;;\; x = \tilde{x}\frac{\lambda}{2} \;;\; t = \tilde{t}\frac{D}{V_0^2} \;;\; Le = \frac{\alpha_L}{D} \;;\; N = \begin{cases} \frac{\alpha_S}{\alpha_L} & solid \\ 1 & liquid \end{cases} \qquad (1)$$

$$A = \frac{2D}{V_0\lambda} \;;\; B = \begin{cases} 0, & lamellar\ structure \\ 1, & rod\ structure \end{cases}$$

The non-dimensional equations then have the form:

$$\frac{\partial C}{\partial \tilde{t}} = \frac{\partial^2 C}{\partial \tilde{z}^2} + A^2 \frac{\partial^2 C}{\partial \tilde{x}^2} + BA^2 \frac{1}{\tilde{x}} \frac{\partial C}{\partial \tilde{x}}$$
$$\frac{\partial T}{\partial \tilde{t}} = NLe \frac{\partial^2 T}{\partial \tilde{z}^2} + NLeA^2 \frac{\partial^2 T}{\partial \tilde{x}^2} + NLeBA^2 \frac{1}{\tilde{x}} \frac{\partial T}{\partial \tilde{x}} \quad (2)$$

Since the thermal and mass boundary layers are quite different for growth from the melt, we use a transformation of variables. This is done in order to be able to distinguish the weak variations of solute concentration at the interface and to have the whole thermal boundary layer in the computational domain without increasing the number of computational elements. We use the transformation:

$$\eta = 1 - \exp\left(-\gamma\left[\tilde{z} - \tilde{I}(\tilde{t})\right]\right) \quad ; \quad \xi = \tilde{x} \quad ; \quad \tau = \tilde{t} \quad (3)$$

The Jacobian of the transformation has the form:

$$J = \begin{bmatrix} 1 & 0 & 0 \\ 0 & \gamma(1-\eta) & 0 \\ 0 & -\tilde{I}_t & 1 \end{bmatrix} \quad (4)$$

The governing equations become:

$$\frac{\partial C}{\partial \tau} = \gamma^2 (1-\eta)^2 \frac{\partial^2 C}{\partial \eta^2} + \left[\tilde{I}_t \gamma - \gamma^2\right](1-\eta)\frac{\partial C}{\partial \eta} + A^2 \frac{\partial^2 C}{\partial \xi^2} + BA^2 \frac{1}{\xi}\frac{\partial C}{\partial \xi}$$
$$\frac{\partial T}{\partial \tau} = NLe\gamma^2 (1-\eta)^2 \frac{\partial^2 T}{\partial \eta^2} + \left[\tilde{I}_t \gamma - Le\gamma^2\right](1-\eta)\frac{\partial T}{\partial \eta} + NLeA^2 \frac{\partial^2 T}{\partial \xi^2} + NLeBA^2 \frac{1}{\xi}\frac{\partial T}{\partial \xi} \quad (5)$$

where equation (5) for the temperature has to be solved in both liquid and solid phases.

One limitation of the above method is that when the interface becomes highly branched, the generation of a boundary-conforming grid is a very difficult task. Furthermore, in the event of topological changes, such as a merger or break-up of the growth interfaces, the boundary fitted grid has to be rearranged. Thus, there is a need to 'decouple' the motion of the interface from the grid motion.

There are three primary restrictions on interface tracking. First, there is the possibility of fragmentation or merger of interfaces. The generation of a body-fitted grid is useless in this case. Second, the function describing the interface needs to be obtained very accurately, since inaccuracy leads to large errors in the first and second derivatives that are used in the domain transformation. The boundary conditions need to be imposed at the exact location of the interface separating the two phases.

Phase-field model

In order to be able to track the interface dynamics, and mainly the region of three phases (liquid and two solid phases) in the eutectic solidification problem, we initially chose the phase-field method. The general approach of the method is a non-equilibrium Cahn-Hilliard [23] diffuse representation of the interface coupled to a diffusion equation. The ideas of Fix [24] were to replace the dynamics of the boundary by an equation of motion for the phase-field, an order parameter that changes from one value to another quickly but smoothly at the two-phase interface. In other words, the phase-field model is a phenomenological model of phase transitions that can be described by a non-conserved scalar order parameter coupled to a conserved non-critical scalar (thermal, concentration) field(s).

The phase field ϕ is governed by a partial differential equation that guarantees that (in the limit of infinitely thin interface region) the appropriate boundary conditions at the crystal/melt

interface are satisfied. One solves the coupled equations for the phase field and transport equations (temperature and/or composition). The advantage of the phase-field formulation of solidification is that no distinction is made between the solid, liquid, and interface. This allows the whole domain to be treated in the same way numerically. The interface is not tracked but, rather, is given implicitly by a scalar function of space and time. This scalar function is called the phase field parameter. This approach readily allows computation of the evolution of interfacial structures, but at the expense of computer time. (We are immensely grateful to Barbara Facemire for arranging the use of the supercomputer at Marshall Space Flight Center for these computations.)

Let $\phi(\mathbf{r},t)$ be the phase-field parameter, a function of the space variable $\mathbf{r}$ within a finite volume, and time t. Its evolution equation in the Ginzburg-Landau approach is:

$$\frac{\partial \phi}{\partial t} = -\frac{1}{\tau}\left(\frac{\delta F(\phi)}{\delta \phi}\right) \tag{6}$$

where τ is an interface kinetic coefficient and F is the Helmholtz free energy. This equation sets the microscopic time scale for order-parameter relaxation and assumed to be independent of ϕ. Hereafter, we assume that there is no volume change in the system subjected to the phase transition dynamics. Everything holds at constant pressure.

The free energy is chosen to have two minima, corresponding to two definite phases at equilibrium. It is represented by the Cahn-Hilliard [23] term $g(\phi)$ and a non-equilibrium driving term $f_0(\phi)$, which is the bulk free energy density and is phase-dependent:

$$F(\phi) = \int_{\Omega^n} [Tg(\phi) + f_0(\phi)] d^n \vec{r} \tag{7}$$

The term $g(\phi)$ is given by the Taylor expansion about the free energy density of the uniform phase-field in an isotropic medium:

$$g(\phi) = g_0(\phi) + \frac{\varepsilon^2}{2}(\nabla \phi)^2 \tag{8}$$

Therefore, the representation of the free energy density in the Cahn-Hilliard form (23) reveals that the free energy density can be expressed as the sum of two contributions: one for the homogeneous phase and the other (gradient energy) as a function of the local properties. The local form of g_0 must have two quadratic minima, corresponding to the two different phases, i.e. the two different values of ϕ. We took ϕ in the minima to be (-1,1). In this case, g_0 is defined by $g_0(\phi)=(1/4)\ W\ (1-\phi^2)^2$ in the Landau-Ginzburg model. The form of g_0 is a double-well potential, as used by Cahn and Hilliard.

For a eutectic alloy we must choose another phase field parameter to be able to differ not only between solid and liquid, but also between the two solid phases [25]. The phases are defined in such a way that:

$$\begin{array}{lll} \alpha - phase & \phi = -1 & \psi = 1 \\ \beta - phase & \phi = -1 & \psi = -1 \\ liquid\ phase & \phi = 1 & \psi - undefined \end{array} \tag{9}$$

We let the mole fraction of component-1 in the parent phase 2 be x. The free energy density of the solution was taken to be phase- and composition-dependent. It describes the change in free energy density in the range of two pure components at thermodynamic equilibrium (solid or liquid phase):

$$f(\phi,\psi,x,T)=\frac{RT}{v_m}[x\ln x+(1-x)\ln(1-x)]$$
$$-(1-h(\phi))\{h(\psi)[xF_1^{\alpha}(T)+(1-x)F_2^{\alpha}(T)]+(1-h(\psi))[xF_1^{\beta}(T)+(1-x)F_2^{\beta}(T)]\} \quad (10)$$
$$+\frac{1}{4}\{h(\psi)W^{\alpha L}+(1-h(\psi))W^{\beta L}\}Tg(\phi)+\frac{1}{4}(1-h(\phi))W^{\alpha\beta}Tg(\psi)$$

where h(ϕ), h(ψ), g(ϕ) and g(ψ) are polynomial functions of the phase-field. In equation (10), R is the universal gas constant and v_m is the molar volume (assumed to be constant and the same for both components. The first term is the free energy density associated with the mixing of two components assuming an ideal solution. The F in the second two terms are associated with the energy density due to individual Helmholtz free energy density of the pure components:

$$F_1^{\alpha}(T)=\Delta H_1\left(1-\frac{T}{T_1}\right);F_2^{\beta}(T)=\Delta H_2\left(1-\frac{T}{T_2}\right) \quad (11)$$

where ΔH_i is the latent heat (enthalpy of fusion) of pure component i and T_i is its melting point. We also assumed for simplicity that the interface properties, i.e. the interface free energy σ and the effective width δ of the interface are weak functions of composition. This means that the phase-field parameters are also independent of composition field. The same concerns the relaxation parameter τ. The phase-field parameters, ε and W, and the relaxation parameter τ, are related to the interfacial energy σ, the interface thickness δ, and the interface mobility μ by:

$$\varepsilon=\frac{\sqrt{3\sigma\delta}}{2\sqrt{2}};W=\frac{3\sigma}{\delta};\tau=\frac{3\sqrt{2}\sigma\delta T}{8\mu T_E} \quad (12)$$

For simplicity, we used the relaxation parameter at the eutectic temperature $T=T_E$. The free energy difference between the phases (for pure solids) is in the excess free energy of phase transformation, and is directly related to the latent heat. The evolution equations for the phase field, composition and enthalpy are given by:

$$\frac{\partial\phi}{\partial t}=\frac{1}{\tilde{\tau}}\left[-\frac{1}{T}\frac{\delta F(\phi,\psi,x,T)}{\delta\phi}\right]$$
$$\frac{\partial\psi}{\partial t}=\frac{1}{\tilde{\tau}}\left[-\frac{1}{T}\frac{\delta F(\phi,\psi,x,T)}{\delta\psi}\right]$$
$$\frac{\partial H}{\partial t}=-\nabla\left\{K(\phi,\psi)T^2\nabla\left(\frac{1}{T}\right)\right\} \quad (13)$$
$$\frac{\partial x}{\partial t}=-\nabla\left\{\frac{D(\phi)v_m}{R}x(1-x)\cdot\nabla\left[\frac{\Delta\mu(\phi,\psi,x,T)}{T}\right]\right\}$$

where $\tilde{\tau}=\tau/T_E$, H is the enthalpy, D(ϕ) is the mass diffusivity of the two component solution, and K(ϕ,ψ) is the thermal conductivity. The values of these quantities are different for solid and liquid, i.e. phase-dependent. However, we assumed that the thermal conductivity is the same for both liquid and solid phases, i.e. K(ϕ,ψ) =K. On the other hand, there is a large difference between the solute diffusivities in the solid and the liquid. This means that D depends on the order parameter ϕ. The simple form for solute diffusivity was used:

$$D(\phi)=h(\phi)D_{liquid}+(1-h(\phi))D_{solid} \quad (14)$$

RESULTS

One-sided sharp interface model

Initially, the freezing rate has been specified. (Later we will calculate it as part of the problem.) The temperature distribution was ignored completely, as well as its effect upon physical parameters such as viscosity. The fluid flow through the interface due to growth was accounted for by assuming it fluctuates about the average value. Following the Jackson–Hunt analysis [26], the concentration at the freezing interface in the melt was averaged over the interface area of each phase. Calculations were done for the three eutectic systems shown below.

Systems used for initial calculations with an oscillatory planar freezing front.

System (α-β)	Type	T_{eut}, C	X_{eut} (β)	$X_\alpha(\beta)$	$X_\beta(\beta)$	m_α,* K/at.frac	m_β,* K/at.frac	T_α, C	T_β, C
Cd - Zn	lamellar	266	0.266	0.0435	0.9875			312	419
Pb - Sn	lamellar	183	0.739	0.29	0.986	395	136	327	232
MnBi-Bi	rod	262	0.978	~0.5	~1	415	218	-	271

Solution of the first equation in (5) gives the interfacial melt concentration, which varies with time. These oscillations of concentration propagate into the bulk of the melt with decaying amplitude. The concentration maxima do not coincide with the maxima of the freezing rate, but lag behind, with a phase difference between the oscillations in freezing rate and in concentration. At high frequencies, the phase difference is several orders of magnitude higher than the inverse diffusion time defined in (1). The concentration at the interface can be averaged separately for each solid phase, yielding results as exemplified by Figure 1.

The spatially averaged concentration along the interface can be temporally averaged by integrating over one period of freezing rate oscillations:

$$\overline{C} = \frac{\int_0^{2\pi} C(t)\cdot V(t)dt}{\int_0^{2\pi} V(t)dt} \tag{15}$$

These doubly averaged concentrations reach constant values after a few periods of oscillations (Figure 2). Similar to the one-dimensional oscillatory case, the difference between the averaged concentration over each phase and its steady state value (without freezing rate oscillations) can be expressed as:

$$\Delta C_{(\alpha,\beta)} = \varepsilon\left|C_M - C_m\right|\cos(\phi) = \varepsilon^2\left|C_E - C_{(\alpha,\beta)}\right| f(\omega)\cos(\phi) \tag{16}$$

where ε is the amplitude of growth rate fluctuations, C_M and C_m are the maximum and minimum values of concentration variations respectively, ϕ is the phase lag between concentration and freezing rate oscillations, and $f(\omega)$ is a weak function of the frequency dependence. The frequency dependence of ΔC according to Equation (16) is shown in Figure 3 (solid markers). The open markers show the difference between the spatially averaged concentration (Equation (15)) and the steady state value for each phase. The difference between these estimations is 5-10% of the offset value, due to time averaging of the concentration oscillations.

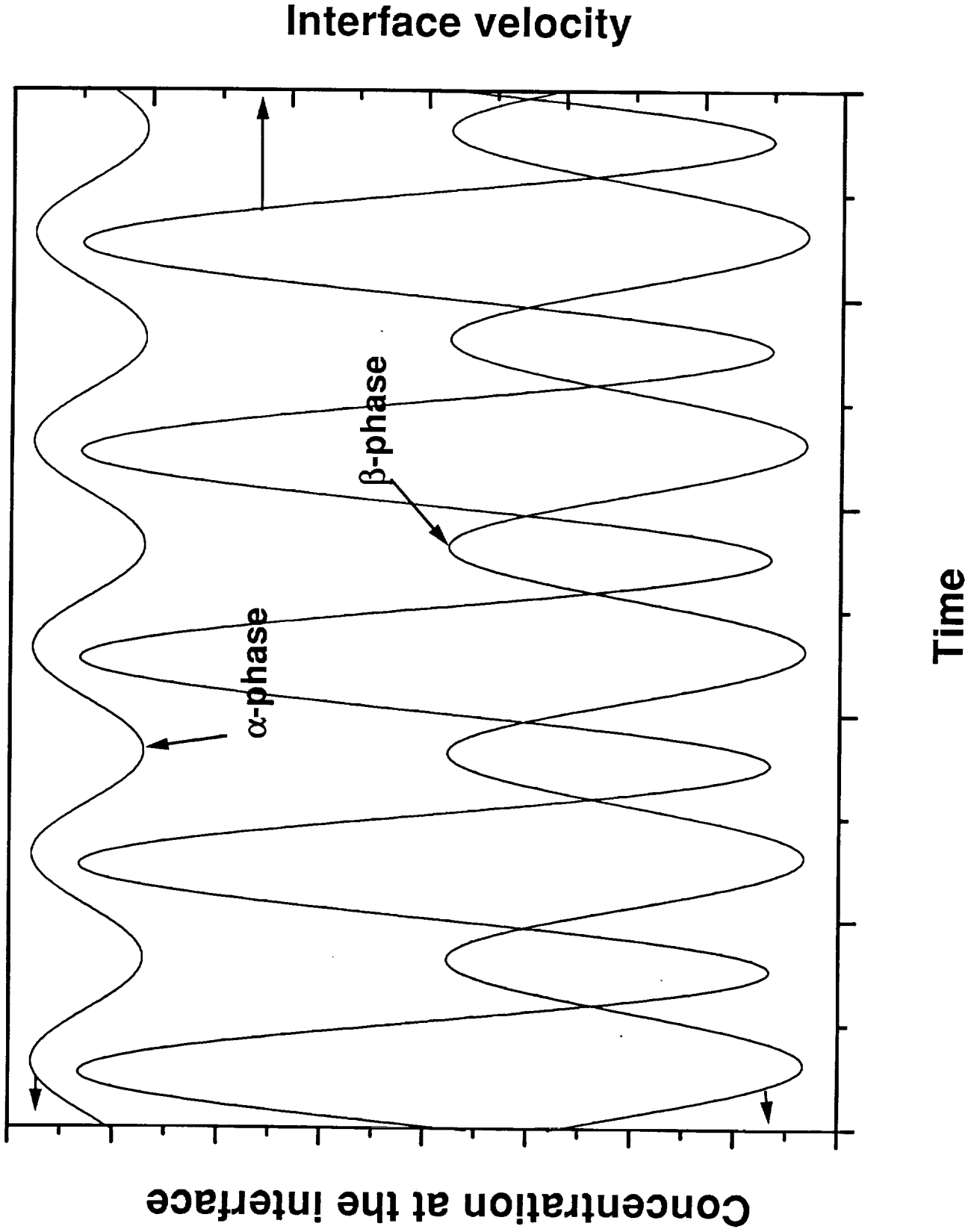

Figure 1. The oscillating freezing rate and the spatially-averaged melt concentrations at the α and β solid phases as a result of the solution of the first equation in (5).

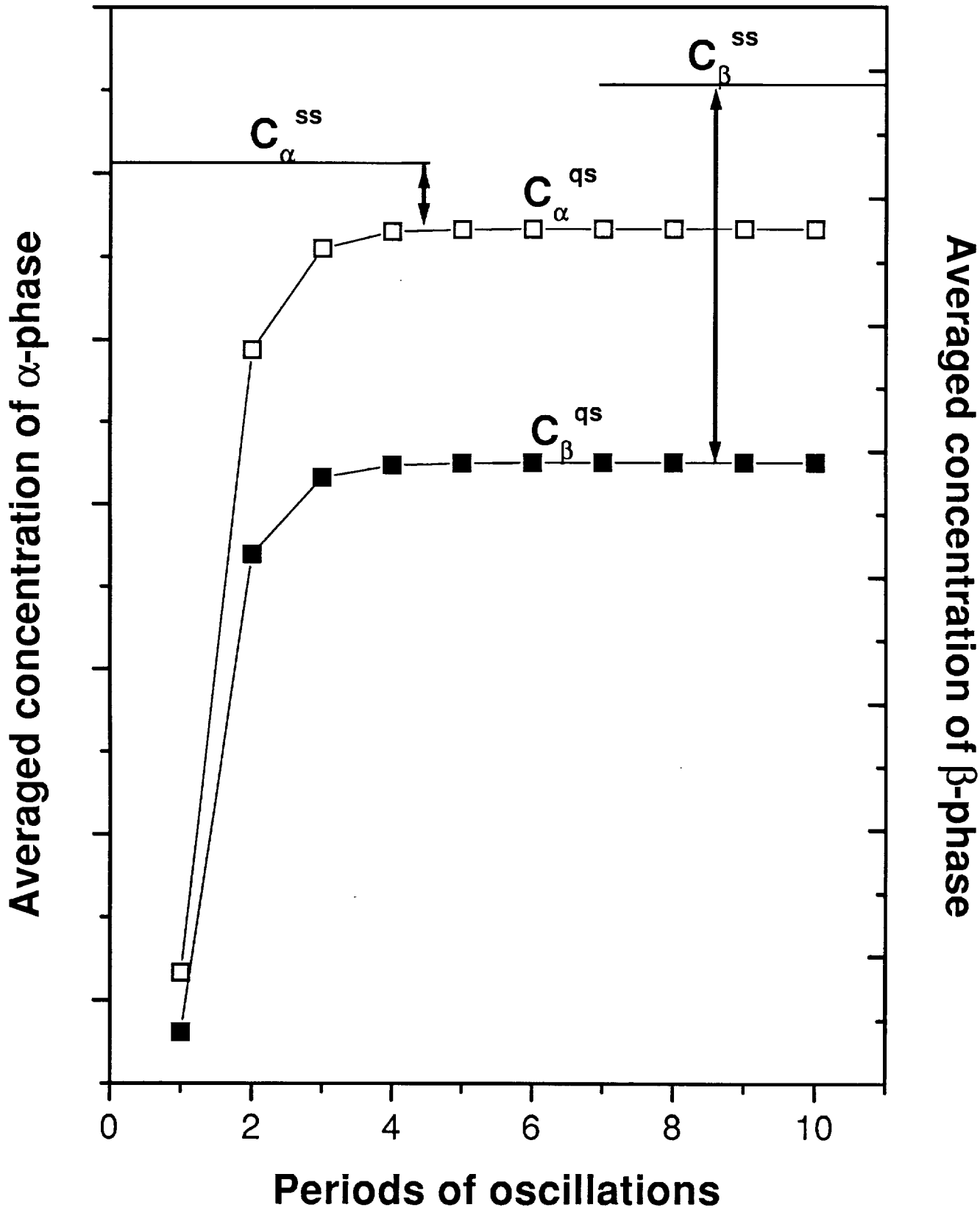

Figure 2. Spatially and temporally averaged concentrations at the freezing interface versus initiation of freezing rate oscillations. Here C_α^{ss} and C_β^{ss} denote the steady-state values without oscillations, and C_α^{qs} and C_β^{qs} are calculated from solution of (5).

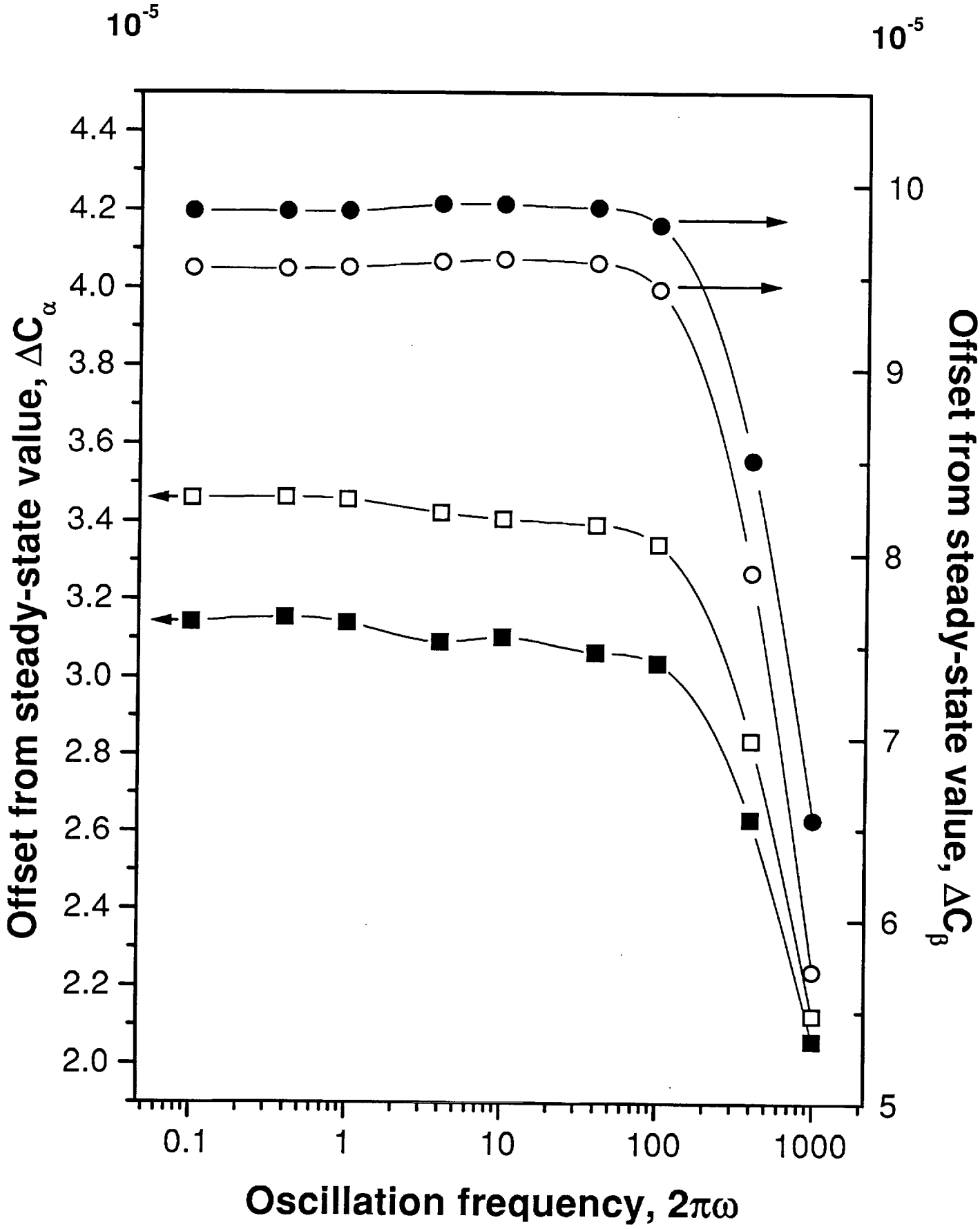

Figure 3. The frequency dependence of the difference $\Delta C_{(\alpha\beta)}$ between the average interfacial concentration with and without freezing rate oscillations. The solid markers are values calculated using Equation (16). The hollow markers were calculated from Equation (15).

The average compositional undercooling ahead of the growing phase is equal to the liquidus slope at the eutectic point times the difference between the average composition and the eutectic. With the freezing rate oscillations applied, the melt ahead of a phase becomes more depleted in the growth component than in the absence of oscillations. To estimate the excess undercooling due to freezing rate oscillations ahead of the growing phase, it is sufficient to know the liquidus slope m_i ($i=\alpha,\beta$) and the difference of the average composition from the eutectic. Two situations are revealed:

1. $|C_\alpha-C_E| < |C_\beta-C_E|$ and $m_\alpha > m_\beta$. Since $\Delta C_\alpha \sim |C_\alpha-C_E|$ and $\Delta C_\beta \sim |C_\beta-C_E|$, the excess undercoolings $\Delta T_\alpha \approx \Delta T_\beta$ (Diagram 1).
2. $|C_\alpha-C_E| < |C_\beta-C_E|$ and $m_\alpha < m_\beta$. Since $\Delta C_\alpha \sim |C_\alpha-C_E|$ and $\Delta C_\beta \sim |C_\beta-C_E|$, the excess undercoolings $\Delta T_\alpha << \Delta T_\beta$ (Diagram 2).

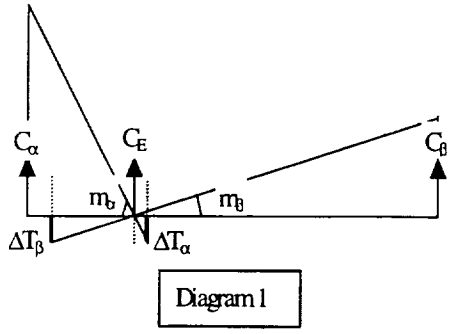

Diagram 1

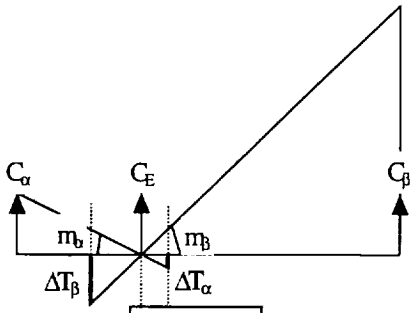

Diagram 2

The average compositional undercooling at the freezing interface varies with the oscillation frequency, and reaches a constant value as frequency is increased. The value of the frequency at which the undercooling becomes constant is proportional to the inverse diffusion time connected with lateral diffusion.

Phase-field model

First, we tried to achieve the necessary accuracy in calculating the concentration in the bulk of the phases, still providing a correct solution for the interfacial region. We solved (13) for one solid phase only, in 1 dimension and constant temperature. Neumann boundary conditions were imposed at the boundaries for the phase-field and mass transport equations. Dirichlet boundary conditions were implemented for heat transport. An explicit Euler scheme was used for time integration.

To find the equilibrium solid and liquid concentrations (exact solutions), we used the criteria for the chemical potentials in the two-component, 2-phase system:

$$\Delta\mu = \mu_1^S - \mu_2^S = \mu_1^L - \mu_2^L \quad \Rightarrow \quad \left.\frac{\partial f_S}{\partial x}\right|_{x_S} = \left.\frac{\partial f_L}{\partial x}\right|_{x_L}$$
$$\mu_2^S = \mu_2^L \quad \Rightarrow \quad f_S - x_S \left.\frac{\partial f_S}{\partial x}\right|_{x_S} = f_L - x_L \left.\frac{\partial f_L}{\partial x}\right|_{x_L} \qquad (17)$$

The first equation in (17) guarantees that at equilibrium the difference in chemical potentials between the two components in one phase is the same as in the second phase. The second condition is that the chemical potential for each component must be the same in both phases.

These two equations are both necessary and sufficient for a solution to exist. Here:

$$\ln\frac{x_L}{x_S}=-\frac{\Delta F_1 v_m}{RT} \quad ; \quad \ln\frac{1-x_L}{1-x_S}=-\frac{\Delta F_2 v_m}{RT} \tag{18}$$

which represents the system of coupled nonlinear equations for x_S and x_L. This system can be solved analytically [27] and results in:

$$x_L=\frac{-1+\exp\left(\frac{\Delta F_2 v_m}{RT}\right)}{\exp\left(\frac{\Delta F_1 v_m}{RT}\right)-\exp\left(\frac{\Delta F_2 v_m}{RT}\right)};x_S=\frac{\left(-1+\exp\left(\frac{\Delta F_2 v_m}{RT}\right)\right)\exp\left(\frac{\Delta F_1 v_m}{RT}\right)}{\exp\left(\frac{\Delta F_1 v_m}{RT}\right)-\exp\left(\frac{\Delta F_2 v_m}{RT}\right)} \tag{19}$$

The following results from the numerical computations were compared to exact solutions (19). In the first try, the simplest form of the finite-difference approximation to the governing equations was chosen, first-order central differencing. The first-order central difference uses the following representations of the first and second derivatives for the composition:

$$\frac{dx}{dz}=\frac{x_{i+1}-x_{i-1}}{2\Delta x};\frac{d^2x}{dz^2}=\frac{x_{i+1}-2x_i+x_{i-1}}{\Delta x^2} \tag{20}$$

The calculations were carried out for several values of temperature. The results are summarized below.

First-order central difference results

T, K	x_S exact	x_L exact	x_S calcul.	x_L calcul.	dx_S error%	dx_L error%	k exact	k calcul	dk error %
610	0.9772	0.9926	0.9065	0.9678	-7.24	-2.50	0.984	0.938	-4.85
650	0.8917	0.9597	0.8350	0.9350	-6.36	-2.57	0.929	0.893	-3.89
800	0.6249	0.7936	0.6013	0.7768	-3.77	-2.12	0.787	0.774	-1.69
1000	0.3278	0.4805	0.3348	0.4885	2.13	1.67	0.682	0.685	0.47
1100	0.1874	0.2894	0.2032	0.3105	8.43	7.29	0.648	0.654	1.07
1150	0.1176	0.1858	0.1374	0.2142	16.83	15.29	0.633	0.642	1.34
1200	0.0477	0.0770	0.0746	0.1187	56.41	54.16	0.620	0.629	1.37
1230	0.0056	0.0092	0.0153	0.0246	173.21	167.39	0.613	0.624	1.83

The error estimate for x_S and x_L was made by the formula:

$$\delta x_S=\frac{x_S^{(calculated)}-x_S^{(exact)}}{x_S^{(exact)}}\cdot 100\% \quad ; \quad \delta x_L=\frac{x_L^{(calculated)}-x_L^{(exact)}}{x_L^{(exact)}}\cdot 100\% \tag{21}$$

The same formula was used for the calculation of the error in segregation coefficient k, where

$$k^{(exact)}=\frac{x_S^{(exact)}}{x_L^{(exact)}} \quad ; \quad k^{(calculated)}=\frac{x_S^{(calculated)}}{x_L^{(calculated)}} \tag{22}$$

The estimates for the solidus, liquidus, equilibrium concentrations and segregation coefficient show relatively large errors, especially near the melting points of the pure components (600 and 1234 K).

In order to improve the accuracy of the numerical result, second order central differencing was also implemented. The second-order central difference uses the following representations of the first and second derivatives for the composition:

$$\frac{dx}{dz} = \frac{-x_{i+2} + 8x_{i+1} - 8x_{i-1} + x_{i-2}}{12\Delta x}; \frac{d^2x}{dz^2} = \frac{-x_{i+2} + 16x_{i+1} - 30x_i + 16x_{i-1} - x_{i-2}}{12\Delta x^2} \quad (23)$$

These results are summarized below.

Second-order central difference results.

T, K	x_S exact	x_L exact	x_S calcul.	x_L calcul.	dx_S error%	dx_L error%	k exact	k calcul	dk error %
610	0.9772	0.9926	0.9656	0.9888	-1.19	-0.38	0.984	0.977	-0.80
650	0.8917	0.9597	0.8893	0.9588	-0.27	-0.09	0.929	0.928	-0.17
800	0.6249	0.7936	0.6240	0.7930	-0.14	-0.08	0.787	0.787	-0.06
1000	0.3278	0.4805	0.3279	0.4806	0.03	0.02	0.682	0.682	0.02
1100	0.1874	0.2894	0.1879	0.2902	0.27	0.28	0.648	0.648	0
1150	0.1176	0.1858	0.1184	0.1869	0.68	0.59	0.633	0.634	0.08
1200	0.0477	0.0770	0.0487	0.0789	2.10	2.47	0.620	0.620	0.05
1230	0.0056	0.0092	0.0059	0.0096	4.64	3.91	0.613	0.613	0.02

The accuracy of the calculations was dramatically improved, especially for temperatures close to the melting points of the pure components. We used 300 grid points in the calculations. Any further increase in the density of grid points seemed to be unnecessary, as seen by comparison of the accuracy of calculations for 100, 200 and 300 grid points. Figure 4 shows how the concentration takes equilibrium values in liquid and solid phases, satisfying equation (13) for the phase field ϕ and concentration x for T=1000 K. Superscript 'ini' in the figure denotes the initial value of solute concentration (assumed constant), and superscript 'eq' means the equilibrium solution.

After equilibrium conditions had been obtained, the temperature at the solid end of the computational domain (where ϕ = -1) was lowered, and the temperature of the liquid end was increased. Equilibrium conditions were reached at T = 1200 K. The temperature at the solid end was set to 1198 K, and at the hot end to 1202 K, which gave us a temperature gradient of 100 K/cm (with the length of the computational domain being 0.04 cm). This temperature gradient had to be imposed after the transient process was over. Unfortunately, transient calculations take a long time, so we did not obtain the equilibrium solution. The interface velocity first increases after the temperature is relaxed, then decreases in time approximately by the law $t^{-1/2}$. The concentration at the interface first increases, then begins to decrease, since the freezing rate decreases. When the concentration had almost reached the equilibrium value, the temperature at the hot end of the domain was changed to:

$$T = T_{initial}^{hot} - \left(\frac{dT}{dt}\right)t(1 + \varepsilon \sin(\omega t)) \quad (24)$$

thus specifying an oscillating temperature at the end of the computational domain. Being coupled with the equation for the phase-field parameter and concentration, the time-dependent temperature causes a similar response in the evolution of the phase-field parameter (Figure 5,a,c) and concentration (Figure 5,a,b). The evolution of the phase-field parameter, which looks like a step-function in Figure 5a, determines the dynamics of the boundary. The lines in Figures 5a,c are moving from left to right. The space between these lines is proportional to the velocity of the boundary. In other words, the evolution of the phase-field parameter gives the boundary velocity in the laboratory reference frame. The concentration close to the interface increases with time,

trying to recover the classical exponential profile ahead of a moving interface. Disregarding the oscillations, the velocity of the moving interface first increases, when we started to lower the temperature by the law (24). The freezing rate tends to a constant value as the concentration profile approaches the stationary solution.

We applied the Fourier collocation and Fourier Galerkin methods to phase transition problems in two dimensions using the phase-field model. These methods were chosen in order to be able to describe naturally the temporal evolution of periodic structures such as eutectics. The application to a modified Stefan problem and interphase boundary motion driven by mean curvature were chosen because their phase-field description has received much attention from both mathematical and computational points of view. These phase transition problems were modeled in a two-dimensional periodic shell with no boundary conditions applied explicitly to the governing equations. The periodicity of the structure in two dimensions allows us to decrease the computational domain, e.g. L = $\lambda_{eut.}$, where $\lambda_{eut.}$ is the interlamellar or interrod spacing. We have submitted a paper for publication on the Fourier collocation and Fourier Galerkin methods in the phase-field model [27].

We applied the concepts described in Methods to two-dimensional, three-phase eutectic solidification. Now the free energy density corresponding to the stable phases (solid and liquid) take the form:

$$
\begin{aligned}
f^{L} &= \frac{RT}{v_m}\left[x\ln x+(1-x)\ln(1-x)\right] \\
f^{\alpha} &= \frac{RT}{v_m}\left[x\ln x+(1-x)\ln(1-x)\right]-\left(\Delta F_1^{\alpha}x+\Delta F_2^{\alpha}(1-x)\right) \\
f^{\beta} &= \frac{RT}{v_m}\left[x\ln x+(1-x)\ln(1-x)\right]-\left(\Delta F_1^{\beta}x+\Delta F_2^{\beta}(1-x)\right)
\end{aligned}
\tag{25}
$$

Here F_2^{α} and F_1^{β} were derived using Maple to satisfy the eutectic composition, temperature, and terminal solid composition of both solid phases. The free energy density for each phase at the eutectic temperature is shown in Figure 6. The free energy densities for the solid phases are written with respect to the liquid phase assuming constant heat capacity for all three phases. We solved the system of equations (13) for an initial gradient of temperature between the boundaries of computational domain in growth direction. The eutectic structure adjusts so that the growing interface is in the region of eutectic temperature. Figure 7 shows the slow dynamics of the eutectic structure near the equilibrium position after the temperature field was relaxed. Since the thermal diffusivity is much larger for all phases than the mass diffusivity, the temperature field relaxes almost instantly in the mass diffusion time scale. The β phase (dark) corresponds to small values of concentration x, in agreement with the free-energy curves. In the liquid (gray), the concentration takes intermediate values between the α- and β-phases. The inset of Figure 7 shows the contours of the phase-field parameter ϕ corresponding to the solid/liquid transition. The middle contour line is ϕ=0. The β-phase protrudes into the liquid phase farther than the α-phase, having the larger curvature besides. Since the growth is coupled, the curvature of the β-phase tries to compensate for the large compositional undercooling which appears due to the large composition difference (x_L-x_β) between the bulk liquid and β. The freezing rate slows as the system approaches equilibrium. The phases slowly adjust their volume fractions as they move in the temperature gradient. The interface shape and the composition field ahead of the interface are in agreement with Jackson-Hunt speculations [26].

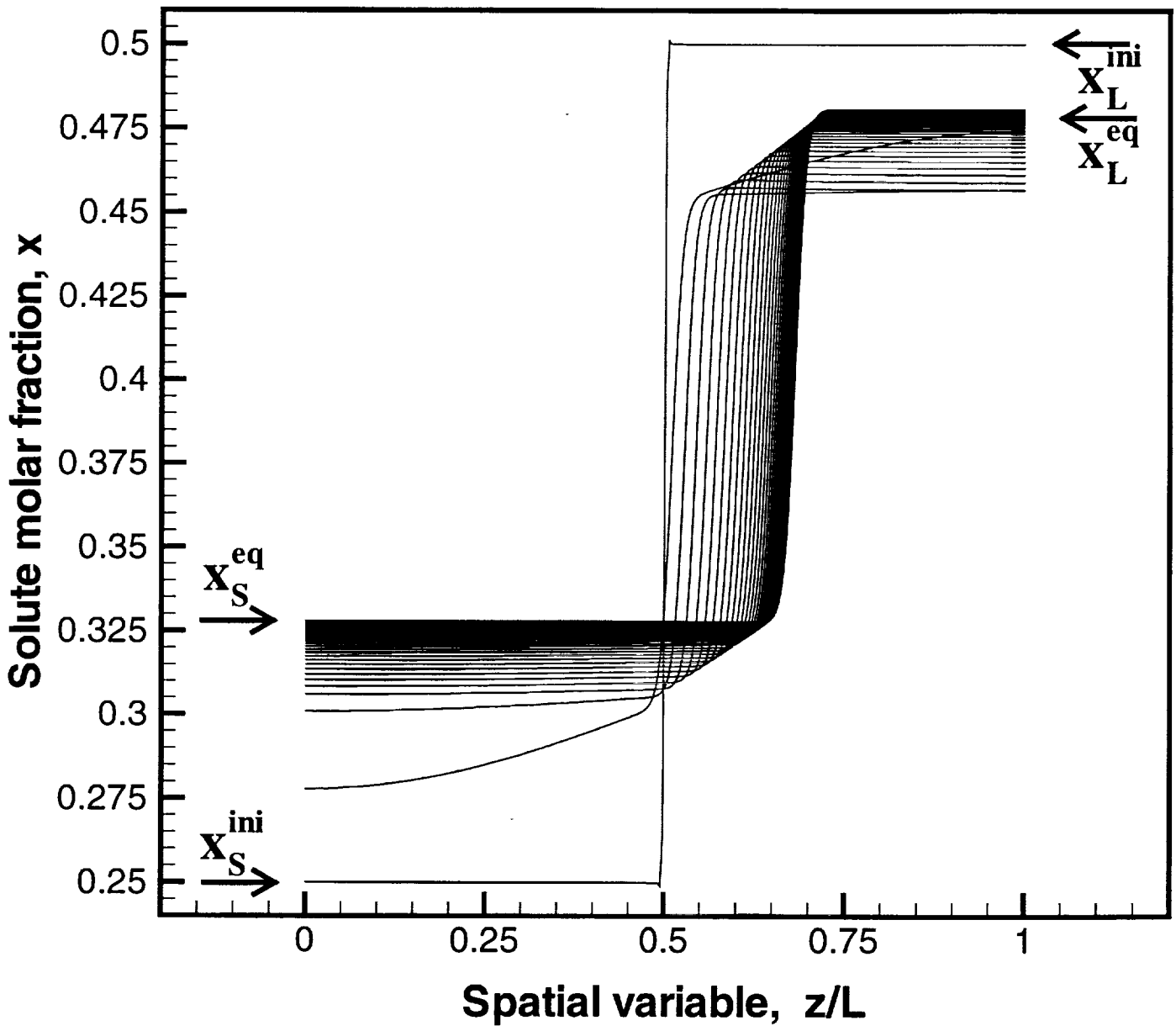

Figure 4. The solution for one-dimensional concentration profile from equation (13) for the phase field ϕ and concentration x at constant temperature T=1000 K.

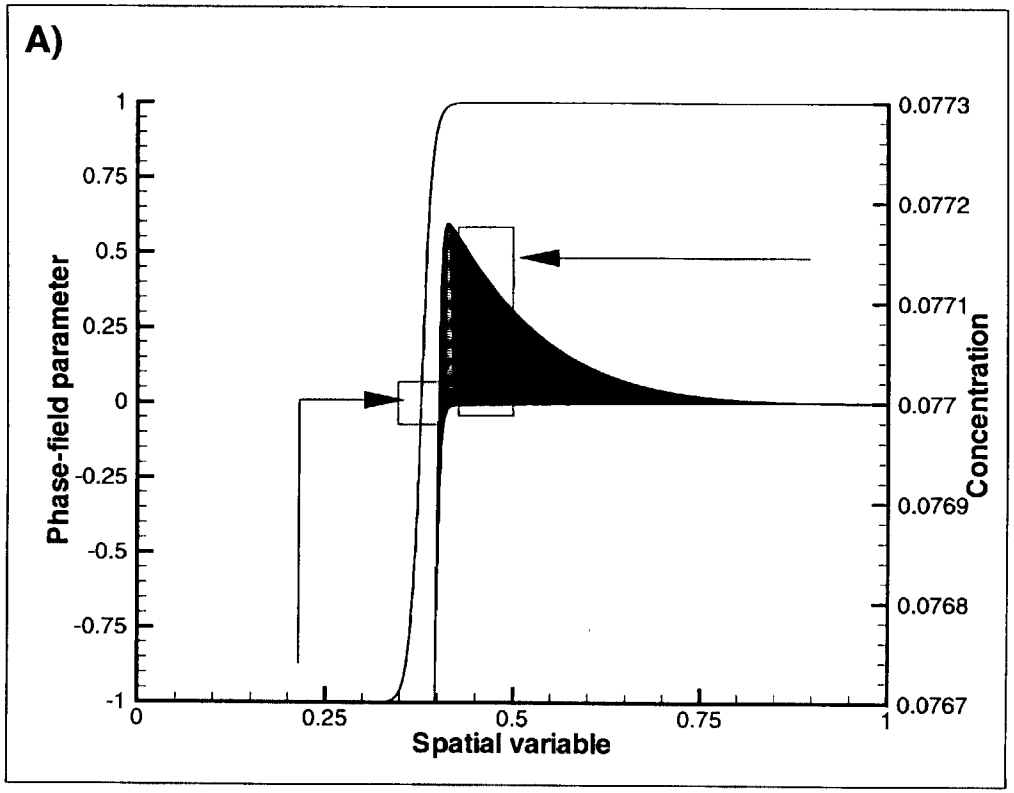

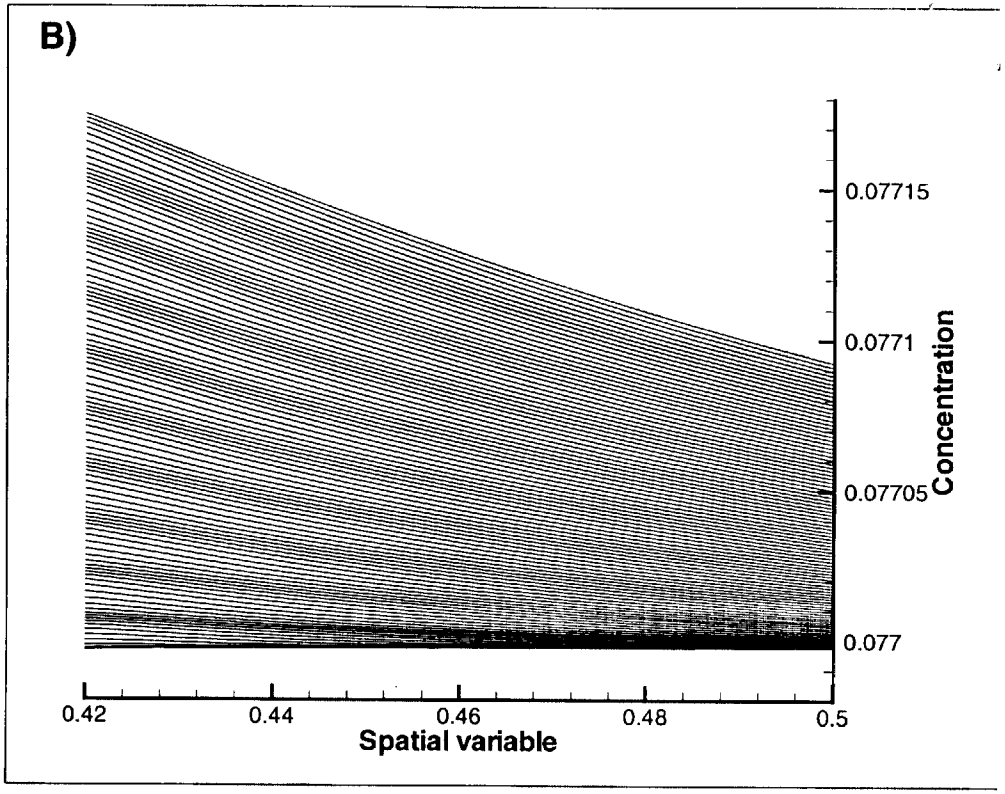

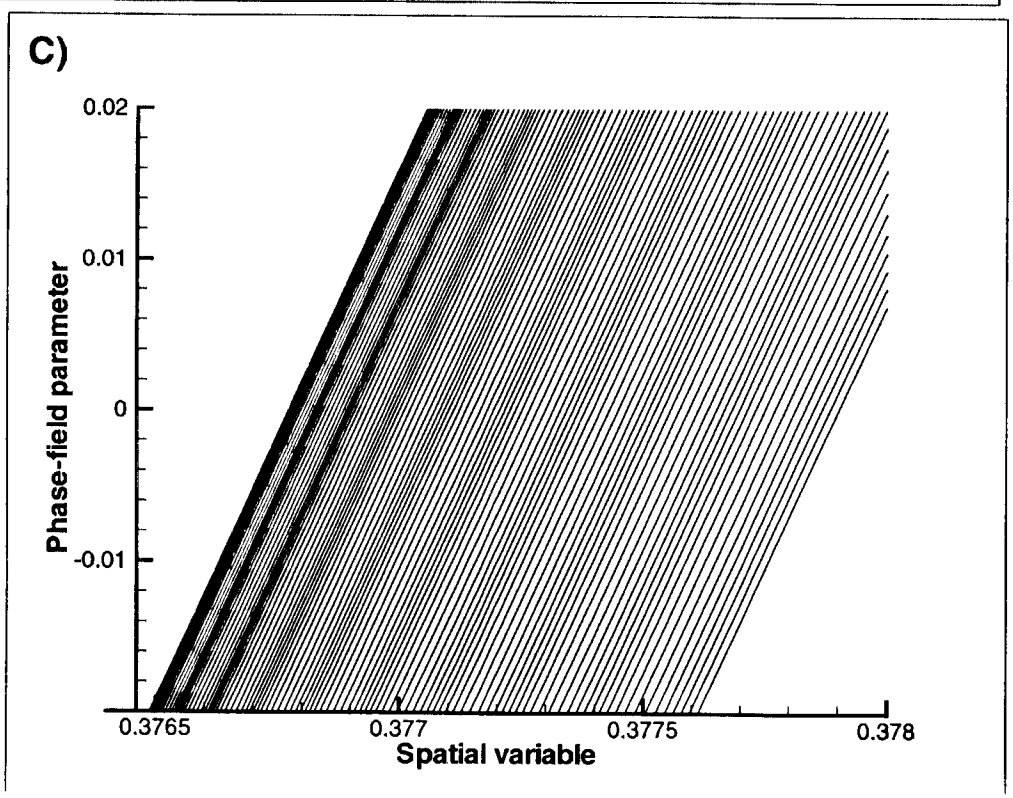

Figure 5. The evolution of the phase-field parameter (A,C) and concentration (A,B) subjected to lowering and oscillating the temperature at the hot end of the computational domain. The evolution of the phase-field parameter, which looks like a step-function in (A), determines the dynamics of the boundary. The lines in (A,C) are moving from left to right; the space between these lines is proportional to the velocity of the boundary.

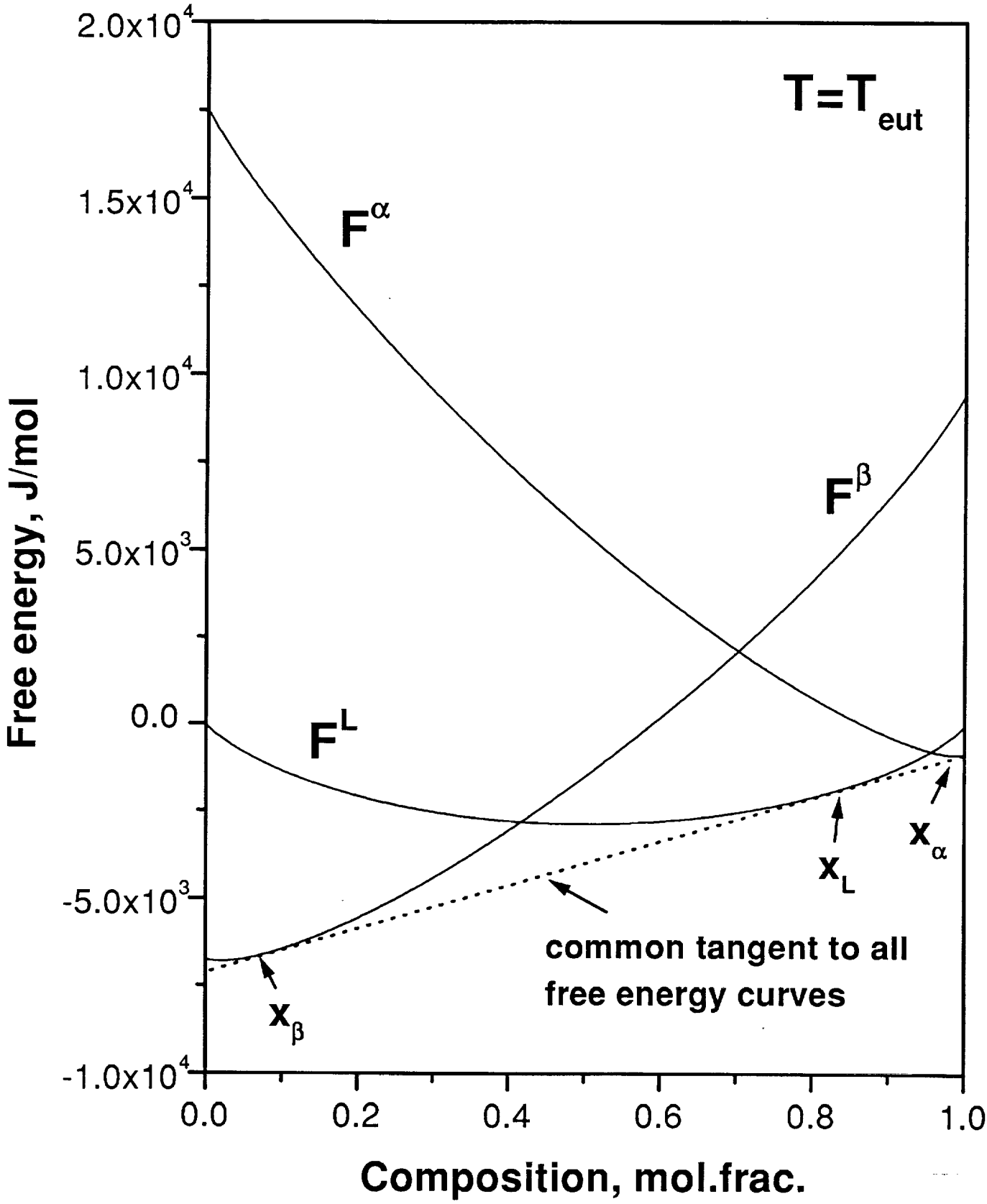

Figure 6. Free energy plot for two solid (F^{α} and F^{β}) and liquid (F^{L}) phase at the eutectic temperature.

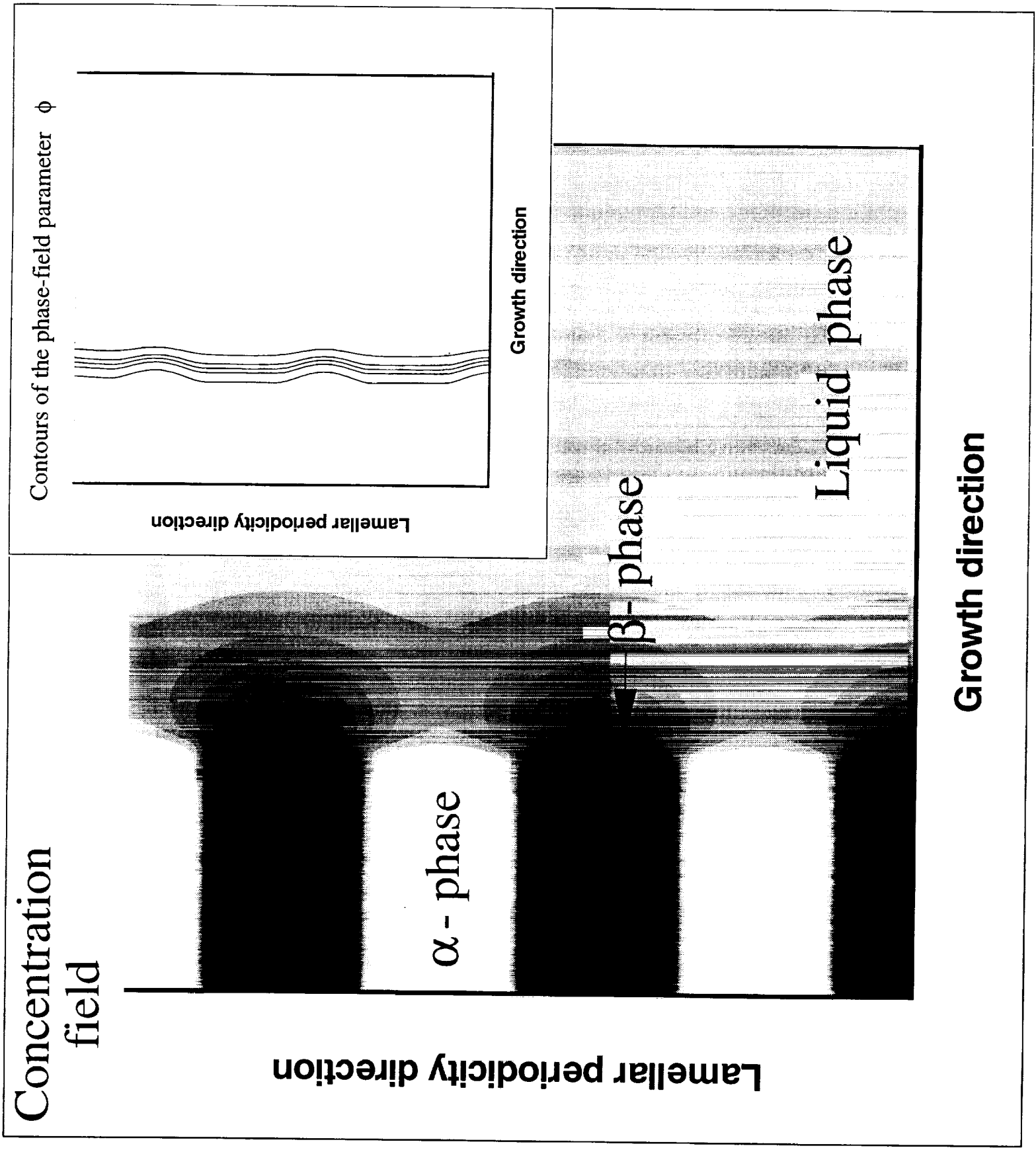

Figure 7. The slow evolution of the eutectic structure towards equilibrium after relaxation of the temperature field. The dark phase (β) corresponds to small values of concentration x. The gray liquid phase concentrations take intermediate values between the α and β solid phases. The inset shows the contours of the phase-field parameter ϕ corresponding to the solid/liquid transition. The middle contour line is $\phi = 0$

PLANS

One-sided sharp interface model

The one-sided model without a temperature field has several shortcomings. The velocity of the moving boundary (the freezing rate) has to be specified. The phases cannot adjust their relative positions. Although the increased undercooling at the interface due to freezing rate oscillations may cause branching of fibers, since the phases are forced to freeze at the same rate, we cannot find which process dominates: branching or termination by overgrowth of the fibers by the matrix. The kinetic undercooling is not consistent with a specified freezing rate.

At present, we are in the process of solving the full system including heat conduction. After the temperature field is obtained, we will set a criterion for nucleation of a branch on a fiber. This nucleation will compete with the ability of the fiber to grow ahead of the matrix. If small undercooling is required for nucleation, then the phase will branch and the eutectic parameter λ will change. Otherwise, one of the phases can protrude in the melt until the criterion for constant growth rate for both phases is reached. No change in λ can result in this case.

Phase-field model

In the phase-field method the steps that were undertaken for the 1-dimensional, 2-phase model should be done for the 2-dimensional, 3-phase eutectic solidification. It may be impossible to completely reach steady-state because the computations require enormous CPU time. To save time, when we determine how the volume fractions adjust when the freezing rate slowly approaches its steady value, we can perturb the freezing by switching on a fluctuating temperature at the hot end of our computational domain. The temperature fluctuations will result in freezing rate and concentration field fluctuations, which will change the eutectic morphology.

DIRECTIONAL SOLIDIFICATION OF Al-Si EUTECTIC

Ramanathan Ramnarayanan

Abstract

The objective of this project is to determine the influence of convection on the microstructure of the Al-Si eutectic. Work began in September 1997 with a literature review. Alumina crucibles encapsulated in quartz were determined to be the most suitable for these experiments and these materials have been purchased. Two Bridgman-Stockbarger furnaces were investigated for use, and one was selected that will permit accelerated crucible rotation for stirring of the melt during solidification. We are in the process of preparing the eutectic alloys and making the growth ampoules.

INTRODUCTION

Al-Si alloys provide 90% of all shaped castings. The reason for its wide acceptance is the attractive combination of its properties such as high corrosion resistance, low coefficient of thermal expansion, fatigue resistance, machinability and good castability. Al-Si alloys have been used for automotive pistons and in the aerospace industry. This system is a faceted-nonfaceted eutectic, so hopefully an understanding of its growth behavior can be extended to other systems of similar structure. Models and theories have been proposed relating to the growth mechanism and effect of freezing rate and impurity modification on the Al-Si eutectic [28-34].

We will study the influence of convection during solidification on the microstructure of the Al-Si eutectic. A Bridgman-Stockbarger apparatus was selected in which the furnace is moved slowly downward and the ampoule can be rotated about its axis.

METHODS

We encapsulate 6mm ID alumina tubes filled with charge in a 10mm ID quartz tube after cleaning both tubes, and alternately evacuating and backfilling with $Ar+H_2$ (10%).

The charge consists of Al-Si (12.6%) by weight. Aluminum shot of diameter 3-5 mm and 99.999% pure will be used. Aluminum contains native oxide which we propose to remove by heating the shot with a solution containing 20g pure chromic acid powder, 35 cm^3 phosphoric acid in 1 liter at 80°C for 1 hr, rinsing with deionized water, drying prior to weighing, and filling the alumina tube. Silicon contains native oxide and some surface impurities which are removed using commercial SC1 solution, rinsing in deionized water, 10%HF for 4 min, rinsing, and drying prior to weighing and filling the alumina tube.

RESULTS

Two Bridgman-Stockbarger apparatuses were investigated for their suitability for the present experiments. We profiled the smaller furnace, used by Fengcui Li for MnBi-Bi, with a K-type thermocouple placed inside a quartz tube of 10 mm ID at three different hot and cold zone temperatures. The results stimulated the following improvements:

1. More insulation was added to the sides to reduce heat loss.
2. A top cover of Fiberfrax insulation was used during profiling to reduce heat loss.

3. The bottom portion of the furnace was fitted with a Mullite tube and a piece of Fiberfrax to prevent air drafts that might induce temperature variations, to prevent tilting of the ampoule, and to reduce the chimney effect.

A larger Bridgman-Stockbarger apparatus was tested and found to be more suitable for the planned experiments. The furnace is moved rather than the ampoule, thus reducing the effects of mechanical vibration on the freezing process. The ampoule is held from below by a support that can be rotated to about 100 rpm, thus permitting use of accelerated crucible rotation to induce convection in the melt.

PLANS

A ceramic separator with a smaller diameter hole may be placed between the top and bottom furnaces constituting the Bridgman-Stockbarger apparatus, in order to provide better control of the freezing interface position. A temperature profile will be obtained by insertion of a thermocouple from above. A support for the growth ampoule will be fabricated from quartz. The Al-Si mixture will be mixed by heating in the growth furnace to above the eutectic temperature, and applying accelerated crucible rotation for a day prior to beginning a solidification run.

After choosing suitable control settings for the top and bottom furnaces, we will grow the eutectic at different growth rates, with and without application of accelerated crucible rotation. The microstructure will be determined by optical microscopy and scanning electron microscopy. The microstructure will be analyzed by commercial image processing software like Adobe Photoshop ® and HLImage++97®.

REFERENCES

1. W.R. Wilcox and L.L. Regel, "Influence of Gravity on the Microstructure of Fibrous Eutectics," Microgravity Quarterly 4, 147-156 (1994).
2. W.R. Wilcox and L.L. Regel, "Influence of Convection on the Microstructure of Fibrous Eutectics," Acta Astronaut. 38, 511-516 (1996).
3. V. Baskaran and W.R. Wilcox, "Influence of Convection on Lamellar Spacing of Eutectics," J. Crystal Growth 67, 343-352 (1984).
4. S. Chandrasekhar, G.F. Eisa and W.R. Wilcox, "Influence of Convection on Lamellar Spacing of Eutectics," J. Crystal Growth 76, 485-488 (1986).
5. R. Caram, S. Chandrasekhar and W.R. Wilcox, "Influence of Convection on Rod Spacing of Eutectics," J. Crystal Growth 106, 194-302 (1990).
6. R. Caram and W.R. Wilcox, "The Soret Effect in Eutectic Solidification," J. Mat. Proc. & Manuf. Sci. 1, 56-68 (1992).
7. J. Seth and W.R. Wilcox, "Effect of Convection on the Microstructure of a Lamellar Eutectic Growing with a Stepped Interface," J. Crystal Growth 114, 357-363 (1991).
8. V. Baskaran, G.F. Eisa and W.R. Wilcox, "Influence of Convection on Eutectic Microstructure," pp. 2-19 in Computational Methods and Experimental Measurements, edited by C.A. Brebbia and G.A. Keramidas, Computational Mechanics Centre, Southhampton.
9. V. Baskaran, I. Ghias and W.R. Wilcox, "Modelling the Influence of Convection on Eutectic Microstructures," p. 115 in Modelling of Casting and Welding Processes II, Metallurgical Society AIME, Warrendale, PA (1984).
10. R.W. Smith, Private Communication, Queen's University, Kingston, Ontario (March 1998).
11. R. Herring, Private Communication, Canadian Space Agency, Montreal (March 1998) .
12. K.A. Jackson and J.D. Hunt, "Lamellar and rod eutectic growth," AIME Trans 236, 1129-1142 (1966)
13. M. Nair, T.W. Fu, W.R. Wilcox, K. Doddi, P.S. Ravishankar and D.J. Larson, D.J., "Response of MnBi-Bi eutectic to freezing rate changes," in: Materials Processing in the Reduced Gravity Environment of Space, pp.533-542, G. E. Rindone, ed., Elsevier (1982).
14. T.W. Fu, W.R. Wilcox and D.J. Larson, "Rate change transients in Bridgman-Stockbarger growth on MnBi/Bi eutectic," J. Crystal Growth 57, 189-194 (1982).
15. T.W. Fu and W.R. Wilcox, "Rate change transients in Bridgman-Stockbarger growth," J. Crystal Growth 51, 557-567 (1981).
16. T.W. Fu and W.R. Wilcox, "Programmed and oscillatory motion in Bridgman-Stockbarger growth," J. Crystal Growth 57, 91-93 (1982).
17. D.T.J. Hurle, E. Jakeman and E.R. Pike, "Striated Solute Distributions Produced by Temperature Oscillations During Crystal Growth from the Melt," J. Crystal Growth 3-4, 633-640 (1968).
18. L.O. Wilson, "The effect of fluctuating growth rates on segregation in crystals grown from the melt: I. No backmelting," J. Crystal Growth 48, 435-450 (1980).
19. A.A. Wheeler, "The effect of a periodic growth rate on the morphological stability of a freezing binary alloy," J. Crystal Growth 67, 8-26 (1984).
20. L.H. Ungar and R.A. Brown, "Cellular Interface Morphologies in Directional Solidification. The One Sided Model," Phys. Rev. B. 29, 1367-1380 (1984).
21. G.B. McFadden and S.R. Coriell, "Non-Planar Interface Morphologies During Unidirectional Solidification," J. Crystal Growth 84, 371-388 (1987).
22. W. Shyy, H.S. Udaykumar and S.J. Liang, "An Interface Tracking Method Applied to Morphological Evolution During Phase Change," Int. J. Heat Mass Transf. 36, 1833-1844 (1993).
23. J.W. Cahn and J.E. Hilliard, "Free energy of a non-uniform system. I. Interfacial free energy," J. Chem. Phys. 28, 258-267 (1958).
24. G.J. Fix, in: Free Boundary Problems: Theory and Applications, vol. II, eds. A. Fasano and M. Primicerio, Pitman, Boston (1983) p.580.
25. A.A. Wheeler, W.J. Boettinger and G.B. McFadden, "Phase-field model for solidification of a eutectic alloy," Proc. Roy. Soc. London, A 452 495-525 (1996).
26. G. Caginalp and J. Jones, "A derivation and analysis of phase-field model of thermal alloys," Annals of Physics 237 66-107 (1995).

27. D.I. Popov, L.L. Regel and W.R. Wilcox, "Fourier Collocation and Fourier Galerkin Methods applied to the Phase-Field Model of Two-Dimensional Phase Transition Problems," J. Physics D: Applied Physics (submitted).
28. http://www.chapmanhall.com/1/jm/jm302230.abs.html
29. L. Clapham and R.W. Smith Acta Met. Mater. **37**, 303 (1989).
30. Magnin et al., ibid **39**,469 (1991).
31. B. Toloui and A. Helawell, Acta Met. **24**, 565 (1976).
32. McLeod and L.M.Hogan, J. Crystal Growth **19**, 301 (1973).
33. M.G. Day and A. Helawell, Proc. Roy. Soc. **305**, 473 (1968).
34. P. Borgeaud et al. AFS C Met. Res. J. **151** (Sept. 1968).